Nitric acid enhancements in the mesosphere during the January 2005 and December 2006 solar proton events

P. T. Verronen,[1] M. L. Santee,[2] G. L. Manney,[2] R. Lehmann,[3] S.-M. Salmi,[1] and A. Seppälä[1,4]

Received 6 April 2011; revised 1 June 2011; accepted 7 June 2011; published 2 September 2011.

[1] We investigate enhancements of mesospheric nitric acid (HNO_3) in the Northern Hemisphere polar night regions during the January 2005 and December 2006 solar proton events (SPEs). The enhancements are caused by ionization due to proton precipitation, followed by ionic reactions that convert NO and NO_2 to HNO_3. We utilize mesospheric observations of HNO_3 from the Microwave Limb Sounder (MLS/Aura). Although in general MLS HNO_3 data above 50 km (1.5 hPa) are outside the standard recommended altitude range, we show that in these special conditions, when SPEs produce order-of-magnitude enhancements in HNO_3, it is possible to monitor altitudes up to 70 km (0.0464 hPa) reliably. MLS observations show HNO_3 enhancements of about 4 ppbv and 2 ppbv around 60 km in January 2005 and December 2006, respectively. The highest mixing ratios are observed inside the polar vortex north of 75°N latitude, right after the main peak of SPE forcing. These measurements are compared with results from the one-dimensional Sodankylä Ion and Neutral Chemistry (SIC) model. The model has been recently revised in terms of rate coefficients of ionic reactions, so that at 50–80 km it produces about 40% less HNO_3 during SPEs compared to the earlier version. This is a significant improvement that results in better agreement with the MLS observations. By a few days after the SPEs, HNO_3 is heavily influenced by horizontal transport and mixing, leading to its redistribution and decrease of the SPE-enhanced mixing ratios in the polar regions.

Citation: Verronen, P. T., M. L. Santee, G. L. Manney, R. Lehmann, S.-M. Salmi, and A. Seppälä (2011), Nitric acid enhancements in the mesosphere during the January 2005 and December 2006 solar proton events, *J. Geophys. Res.*, *116*, D17301, doi:10.1029/2011JD016075.

1. Introduction

[2] High-energy protons emitted from the Sun in coronal mass ejections can cause solar proton events (SPEs) in the Earth's atmosphere. Because of the protection by the Earth's magnetic field, the protons are guided into the polar regions, where they affect locations with magnetic latitudes higher than about 60°. Although relatively infrequent, major SPEs can dramatically increase ionization in the middle atmosphere, typically exceeding the rates due to solar EUV radiation and galactic cosmic rays at 30–90 km altitude. Following the ionization, ion chemical reactions can produce substantial amounts of, e.g., odd hydrogen (HO_x = H + OH + HO_2) and odd nitrogen (NO_x = N + NO + NO_2) [*Porter et al.*, 1976; *Heaps*, 1978; *Solomon et al.*, 1981; *Rusch et al.*, 1981]. Increase in HO_x and NO_x concentration leads to ozone depletion in the mesosphere and upper stratosphere through well-known catalytic reaction cycles [e.g., *Grenfell et al.*, 2006]. Perhaps the most studied major SPE of recent years, at least in terms of ozone changes, is the so-called Halloween event, which occurred in October-November 2003 [e.g., *Seppälä et al.*, 2004; *López-Puertas et al.*, 2005a; *Verronen et al.*, 2005; *Degenstein et al.*, 2005; *Jackman et al.*, 2005; *Rohen et al.*, 2005; *Semeniuk et al.*, 2005; *Funke et al.*, 2011].

[3] Satellite observations made during the Halloween 2003 SPE showed that also many other minor species of the middle atmosphere are affected in the high-latitude regions [e.g., *López-Puertas et al.*, 2005b; *Orsolini et al.*, 2005; *von Clarmann et al.*, 2005]. Of special interest to this study, large amounts of nitric acid (HNO_3) have been observed both during and after SPEs. During an SPE, a high-HNO_3 layer forms at upper stratosphere/lower mesosphere altitudes, and this enhancement typically lasts about one week [*Orsolini et al.*, 2009]. This is the so-called direct HNO_3 effect, which has been attributed to ion-ion recombination taking place after proton impact ionization [*Verronen et al.*, 2008]. On the other hand, the indirect HNO_3 effect is related

[1]Earth Observation, Finnish Meteorological Institute, Helsinki, Finland.
[2]Jet Propulsion Laboratory, California Institute of Technology, Pasadena, California, USA.
[3]Alfred Wegener Institute for Polar and Marine Research, Potsdam, Germany.
[4]British Antarctic Survey, NERC, Cambridge, UK.

0148-0227/11/2011JD016075

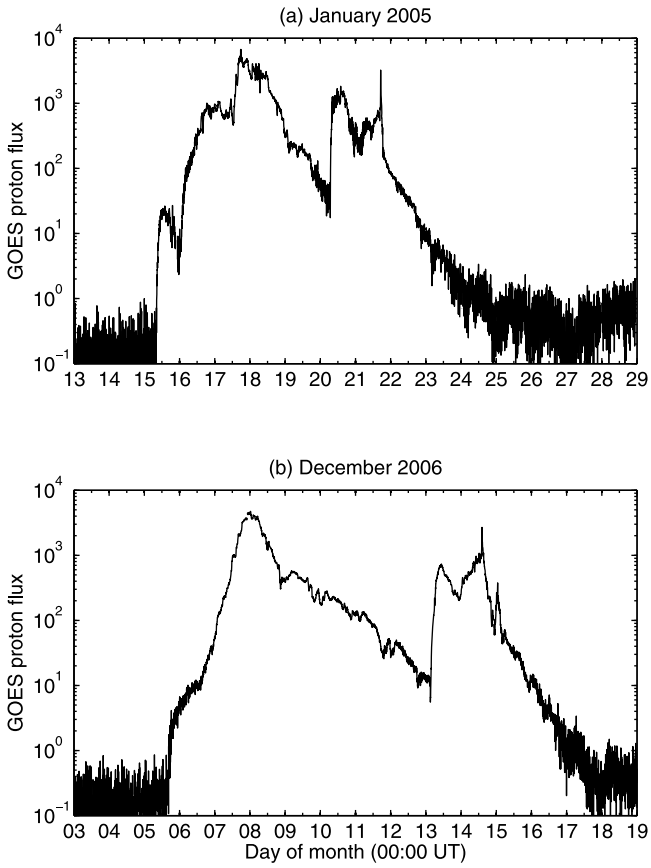

Figure 1. Proton flux observations by GOES-11 at geostationary orbit (cm^{-2} s^{-1} sr^{-1}). Energy range is 5–60 MeV; that is, fluxes of the >60 MeV channel have been subtracted from those of the >5 MeV channel.

to large NO_x amounts which are produced by particle precipitation either in the mesosphere or in the lower thermosphere. The NO_x then descends inside the polar vortex from higher altitudes down to the stratosphere on time scales of months (typically in the spring time). In this case, HNO_3 production occurs gradually in the middle stratosphere, where the descending NO_x is converted to HNO_3 via N_2O_5 [*de Zafra and Smyshlyaev*, 2001; *Stiller et al.*, 2005]. The N_2O_5-to-HNO_3 conversion can be explained by water cluster ion chemistry and heterogeneous reactions on sulphate aerosols.

[4] In the case of the Halloween 2003 SPE, *Verronen et al.* [2008] have already shown that the main process of the direct HNO_3 production is ion-ion recombination between $H^+(H_2O)$ and NO_3^- type ions. In their study, they compared the results of an ion and neutral chemistry model to the observations of the Michelson Interferometer for Passive Atmospheric Sounding (MIPAS/Envisat) instrument. The model predictions of HNO_3 were found to be in good agreement with MIPAS at 70°N, where photodissociation led to strong diurnal variation and rapidly balanced the production by the SPE. However, in the polar night region close to the north pole (85°N), the model overestimated HNO_3 around 60 km by ≈100% compared to MIPAS. *Verronen et al.* [2008] suggested uncertainties of the rate coefficients of the ionic reactions as a possible reason for the excess production.

[5] In this paper, we use the Sodankylä Ion and Neutral Chemistry model (SIC) and extend the study of direct HNO_3 enhancements in the mesosphere. Two events, i.e., the January 2005 and December 2006 SPEs, are analyzed, and the model results are compared with observations by the Microwave Limb Sounder (MLS/Aura) instrument. Because of the disagreement between model predictions and MIPAS observations reported by *Verronen et al.* [2008], we concentrate on polar night regions at very high latitudes (80°N). In the polar night, there is no photodissociation of HNO_3, which would lead to strong diurnal variation and complicate our analysis of HNO_3 production. In addition to the SPE effects, we also discuss the importance of polar vortex dynamics to the observed distribution of HNO_3.

2. SPEs of January 2005 and December 2006

[6] The Geostationary Operational Environmental Satellites (GOES) measure proton fluxes using seven integrated energy channels: >1, >5, >10, >30, >50, >60, and >100 MeV. Protons with such high energies can penetrate the atmosphere down to mesospheric and stratospheric altitudes. However, they are guided by the Earth's magnetic field into the polar regions, so that SPE-related effects are typically confined to magnetic latitudes larger than about 60° [e.g., *Jackman et al.*, 2001; *Rodger et al.*, 2006; *Verronen et al.*, 2007]. Higher energies allow for deeper penetration, so that protons with 5–60 MeV of energy can reach altitudes of approximately 80–45 km, respectively [see, e.g., *Turunen et al.*, 2009, Figure 3].

[7] The proton fluxes observed by GOES-11 at the geostationary orbit are shown in Figure 1. The flux of the >60 MeV channel has been subtracted from that of the >5 MeV channel in order to demonstrate the variation in proton forcing in the upper stratosphere and mesosphere. In January 2005, the SPE begins on day 15, and reaches the peak of flux on day 17 at about 18:00 UT with ≈4000 cm^{-2} s^{-1} sr^{-1}. A second peak of forcing takes place on days 20–21, with fluxes varying between 200 and 2000 cm^{-2} s^{-1} sr^{-1}. The proton flux exceeds 100 cm^{-2} s^{-1} sr^{-1} on days 16–21. In December 2006, the event begins on day 5 and there are two peaks of forcing, on day 8 at about 00:00 UT (≈4000 cm^{-2} s^{-1} sr^{-1}) and on days 13–14 (200–1000 cm^{-2} s^{-1} sr^{-1}). The flux is higher than 100 cm^{-2} s^{-1} sr^{-1} on days 7–10 and 13–14.

[8] Compared to other SPEs, the two events considered here are moderate. SPEs can be ranked according to their magnitude using the peak flux unit *pfu*, which is the flux of >10 MeV protons measured at the geostationary orbit in units cm^{-2} s^{-1} sr^{-1}. The *pfu* of the January 2005 and December 2006 events is 5040 and 1980, respectively (see, e.g., the list of SPEs provided by NOAA Space Environment Services Center at http://www.swpc.noaa.gov/ftpdir/indices/SPE.txt). In contrast, the Halloween 2003 event, which is one of the largest SPEs in the last 45 years, has a *pfu* = 29500. Another method is to rank SPEs after their estimated NO_y production in the middle atmosphere. In the top 15 list of SPEs, the January 2005 event is ranked 11th with 1.8 gigamoles, while the December 2006 event is not

included [*Jackman et al.*, 2008]. Put into perspective, the Halloween 2003 event is ranked 4th with 5.6 gigamoles of NO_y produced. Although not considered an extreme SPE, the January 2005 event had an exceptionally hard spectrum on day 20, i.e., the flux of >100 MeV protons was much higher than that during most SPEs. However, these protons deposit their energy deep in the stratosphere, where at least the direct NO_x and ozone changes related to SPEs, even with such hard spectra, are considered to be relatively small [*Seppälä et al.*, 2008].

3. MLS/Aura Observations

[9] The Microwave Limb Sounder (MLS) instrument is operating on board NASA's Aura satellite, which was launched in July 2004 into a Sun-synchronous near-polar orbit [*Waters et al.*, 2006]. MLS measures thermal emission from the middle atmosphere at millimeter and submillimeter wavelengths that can be inverted into altitude profiles of more than 15 trace gases and temperature. The retrieved species include, e.g., O_3, OH, HNO_3, CO, and H_2O. The instrument can measure in both day and night conditions, and the observations cover geographic latitudes 82°S–82°N on each orbit.

[10] In this study we use MLS L2 data version 3.3. Before the analysis, all MLS data were screened according to the instructions given in the MLS Data Quality and Description Document [*Livesey et al.*, 2011]. To make sure that only night-time data are considered in our study, we selected data with solar zenith angle larger than 100° at the point of measurement.

[11] Considering the HNO_3 observations, the standard MLS/Aura HNO_3 product is a hybrid, formed by merging together retrievals from the 190 and 240 GHz bands [*Santee et al.*, 2007; *Livesey et al.*, 2011]. The "join" level is at 22 hPa (≈25 km), so that at pressures equal to or larger than 22 hPa the data come from the 240-GHz retrievals, whereas at lower pressures the HNO_3 product is taken from the 190-GHz retrievals. The standard recommended altitude range of the observations is between 215 and 1.5 hPa (≈10–50 km), where single-profile precision is 0.7–1.0 ppbv. Retrieved mixing ratios at 1 hPa are also scientifically useful under conditions of HNO_3 enhancement, such as in association with SPE events. Vertical resolution of the HNO_3 observations is 4–5 km in the middle/upper stratosphere up to about 1 hPa, above which it degrades rapidly to ~12 km at 0.1 hPa (≈60 km).

[12] In this work, we use the MLS HNO_3 observations in the upper stratosphere and mesosphere (≈40–80 km, 2.154–0.01 hPa), i.e. data that are outside the generally recommended altitude range [*Santee et al.*, 2007; *Livesey et al.*, 2011]. At these altitudes, the HNO_3 mixing ratios are typically very low, which makes the signal-to-noise ratio of the observations poor. However, in our study we expect that the enhancement of HNO_3 during SPEs leads to improved signal-to-noise ratio and allows us to monitor the changes taking place in the mesosphere. We examined the averaging kernels for the 190-GHz retrievals and found that the observations contain real atmospheric signal up to about 70 km (0.046 hPa), while above that the information content is quite low. Therefore our analysis concentrates on altitudes 40–70 km. It should be noted that the data from these altitudes have not been validated to date, so our study will provide valuable information on the quality of the MLS HNO_3 product in the mesosphere.

[13] In addition to HNO_3, we also use two other data sets to support our discussion of changes in HNO_3 during SPEs: carbon monoxide (CO) and potential vorticity (PV). CO is a long-lived species in the mesosphere, and it is commonly used as a tracer in studies of middle atmospheric dynamics. In the case of the winter polar vortex, high/low CO values typically correspond to regions inside/outside the vortex. The CO data are from the MLS/Aura instrument; see *Pumphrey et al.* [2007] for details on version 2.2 data. Version 3.3 CO mixing ratios are little changed from those in version 2.2, but data quality indicators suggest an improvement in the retrievals [*Livesey et al.*, 2011]. We use also PV as a tool for understanding vortex dynamics. The PV data used here are from the GEOS-5 (Goddard Earth Observing System-Version 5) data assimilation system, described in detail by *Reinecker et al.* [2008]. In the mesosphere, PV often gradually shifts from having highest values near the vortex center (as is the case in the stratosphere) to having them near the edge of the vortex [e.g., *Harvey et al.*, 2009]. In addition, the vortex structure in and above the upper stratosphere is more complex than at lower levels [e.g., *Manney et al.*, 2007]. Mesospheric PV fields from operational meteorological analyses, such as the GEOS-5 fields shown here, have been demonstrated to show significant inaccuracies in some cases [*Manney et al.*, 2008]. Thus, the characterization of the vortex using PV is more complicated in the mesosphere; nevertheless, it can provide information on the extent and position of the vortex.

4. Ion and Neutral Chemistry Modeling

[14] The Sodankylä Ion and Neutral Chemistry (SIC) model combines the complex ion chemistry scheme of the ionospheric D region with the basic chemistry of minor neutral species (e.g., O_x, HO_x, NO_x). The model has been designed specially for studies of ionosphere-atmosphere interaction. Detailed descriptions of SIC have recently been given by *Verronen et al.* [2005] and *Verronen* [2006]. In the following we briefly describe the main characteristics of the model.

[15] The altitude range of SIC is from 20 to 150 km, with 1-km resolution. The model includes a chemical scheme of over 400 reactions, and takes into account external forcing due to solar UV and soft X-ray radiation, electron and proton precipitation, and galactic cosmic rays. The background neutral atmosphere is a combination of the MSISE-90 model [*Hedin*, 1991] and tables given by *Shimazaki* [1984]. The solar flux is estimated by the SOLAR2000 model [*Tobiska et al.*, 2000]. The scattered component of the solar Lyman-α flux is included using the empirical approximation given by *Thomas and Bowman* [1986]. The model includes a vertical transport scheme, as described by *Chabrillat et al.* [2002], which takes into account molecular and eddy diffusion. Within the transport code the molecular diffusion coefficients are calculated according to *Banks and Kockarts* [1973]. The eddy diffusion coefficient

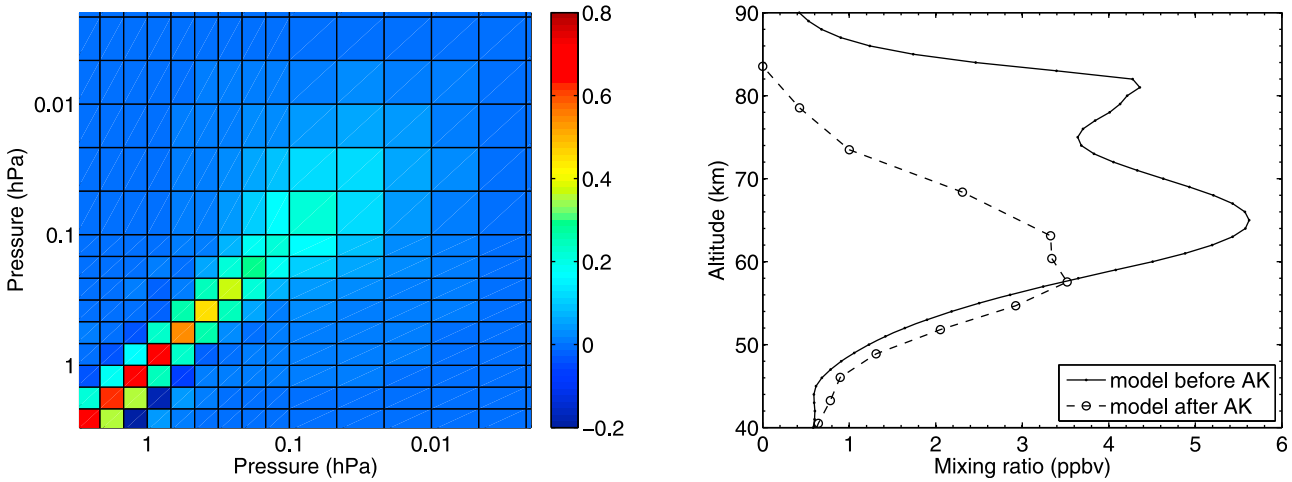

Figure 2. (left) MLS 190-GHz HNO_3 averaging kernels for polar regions. The pressure range is from 3 to 0.002 hPa, which corresponds approximately to altitudes 40–90 km. (right) Example of modeled HNO_3 mixing ratios before and after applying MLS 190-GHz averaging kernels. This example shows a situation where HNO_3 mixing ratios have been significantly increased in the mesosphere by a solar proton event.

profile can be varied, e.g., using the parameterization given by *Shimazaki* [1971].

[16] Ionization rates due to proton precipitation are calculated using GOES-11 satellite proton flux data, available from, e.g., the NOAA National Geophysical Data Center World Wide Web server at www.ngdc.noaa.gov/stp/stp.html. GOES satellites measure integrated proton fluxes above seven threshold values: 1, 5, 10, 30, 50, 60, and 100 MeV. These observations are converted to differential flux spectra using the exponential rigidity relation, and then ionization rates are calculated using the empirical energy-range relation of protons (for details, see *Verronen et al.*, 2005, and references therein].

[17] During SPEs, the most important process producing HNO_3 in the mesosphere, and creating the direct HNO_3 effect, is ion-ion recombination [*Aikin*, 1997; *Verronen et al.*, 2008, and references therein]. HNO_3 is produced through

$$H^+(H_2O)_n + NO_3^-(HNO_3)_m \rightarrow (m+1)HNO_3 + nH_2O \qquad (1)$$

where n and m are integers ranging between 0–8 and 0–2, respectively. In addition to reaction (1), the SIC model includes three other reactions that can increase HNO_3 in the stratosphere during and after SPEs but which have small effects in the mesosphere and are therefore not relevant for this study: 1) N_2O_5 conversion to HNO_3 by ionic reactions, 2) $NO_2 + OH + M \rightarrow HNO_3 + M$, and 3) $NO + HO_2 + M \rightarrow HNO_3 + M$. These reactions are discussed in more detail elsewhere [*Böhringer et al.*, 1983; *de Zafra and Smyshlyaev*, 2001; *Stiller et al.*, 2005; *Butkovskaya et al.*, 2005; *Brühl et al.*, 2007; *Verronen et al.*, 2008].

[18] The ionic production of HNO_3 through reaction (1) is actually a part of the reaction scheme which converts water vapor to HO_x species. *Solomon et al.* [1981] gave a detailed description of how SPEs lead to formation of OH and $H^+(H_2O)_n$ water cluster ions and discussed the subsequent production of H resulting from electron-ion recombination. They pointed out that in the lower mesosphere ion-ion recombination with NO_3^- ions, i.e. reaction (1), was more likely, leading to formation of HNO_3 instead of H. In their study, *Solomon et al.* [1981] focused on the summer pole/solar illuminated conditions and assumed that the HNO_3 thus produced would be photodissociated within hours to release the "missing" H. Therefore, the overall net reaction would still be

$$H_2O \rightarrow OH + H. \qquad (2)$$

[19] However, in polar night conditions HNO_3 has a longer chemical lifetime (~ months), so that after SPEs it can serve as a reservoir of HO_x and be transported from the original location of the proton forcing. This can lead to more effective ozone depletion in the mesosphere because rapid photodissociation of built-up HNO_3 releases HO_x in conditions where atomic oxygen is available for catalytic depletion cycles [*Verronen et al.*, 2006]. Satellite observations have shown that direct HNO_3 enhancements in the mesosphere can be detected for about one week after SPEs [*Orsolini et al.*, 2009], which suggest that the signature of HNO_3 enhancement is diluted through transport and mixing with air unaffected by the SPE.

[20] As pointed out by *Verronen et al.* [2008], the SIC model seems to overestimate the SPE-related production of HNO_3 in the mesosphere. We suspect that this overestimation may arise from the inaccuracy of some reaction rate constants used in the model. To investigate whether this is the case, we analyzed the corresponding reactions. In order to narrow down the list of potential candidates from the hundreds of reactions in the model to less than a dozen reactions, we determined all significant reaction pathways (= reaction sequences) leading to the production of NO_3^-, which is an immediate precursor of HNO_3 according to (1). We used a mathematical algorithm which has been specially designed for analyses of complex chemical systems [*Lehmann*, 2004, 2002]. Applying a fixed ionization rate of 10^3 cm^{-3} s^{-1} (a high but typical rate during large SPEs), we ran the SIC model for 24 hours and then analyzed the nighttime results at 60 km. In this test case, the dominant pathway

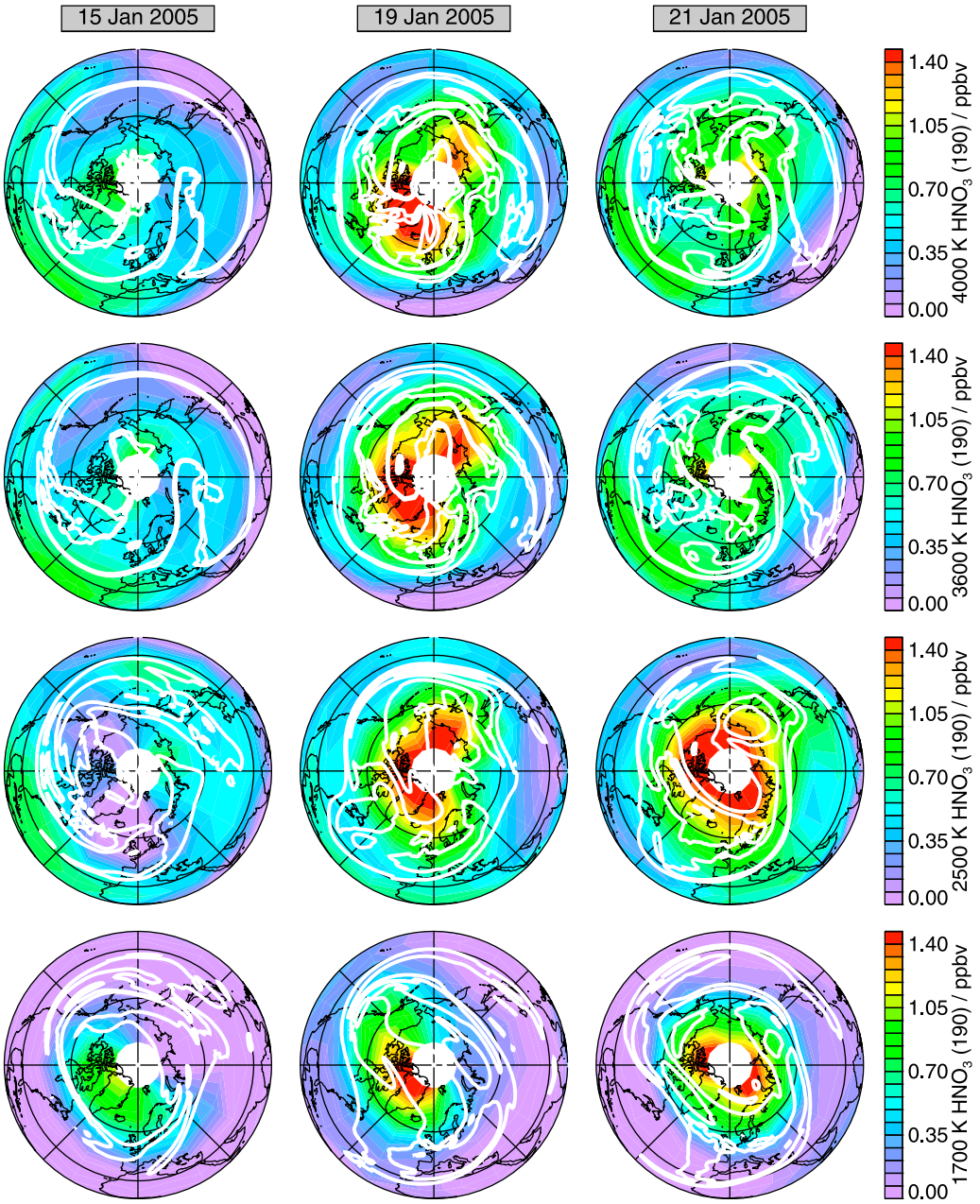

Figure 3. Northern Hemisphere HNO_3 mixing ratios. The data are daily averages of MLS observations at potential temperature surfaces of 1700 K (~50 km), 2500 K (~60 km), 3600 K (~63 km), and 4000 K (~65 km) presented in a 15° × 30° latitude-longitude grid. The precision of the HNO_3 data averaged in these grid boxes ranges from 0.15 to 0.25 ppbv. Note that because of the vertical resolution of the measurements, the HNO_3 values at these levels are not completely independent. The superimposed white lines are potential vorticity contours produced by the GEOS-5 data assimilation system. The PV values, in units of 10^{-4} Km^2 kg^{-1} s^{-1}, at the different levels are: 47 and 85 (1700 K), 235 and 423 (2500 K), 1936 and 2582 (3600 K), and 3006 and 4008 (4000 K).

producing NO_3^- ions from NO_x (= NO + NO_2) is the following one:

$$e^- + O_2 + O_2 \rightarrow O_2^- + O_2 \quad (3)$$

$$O_2^- + O_3 \rightarrow O_3^- + O_2 \quad (4)$$

$$O_3^- + CO_2 \rightarrow CO_3^- + O_2 \quad (5)$$

$$CO_3^- + NO_2 \rightarrow NO_3^- + CO_2 \quad (6)$$

$$\text{Net} : e^- + O_3 + NO_2 \rightarrow NO_3^- + O_2.$$

[21] Here the net reaction consumes ozone and nitrogen dioxide. NO_3^- can then recombine with $H^+(H_2O)_n$ water cluster ions either directly (this is most likely) or after forming

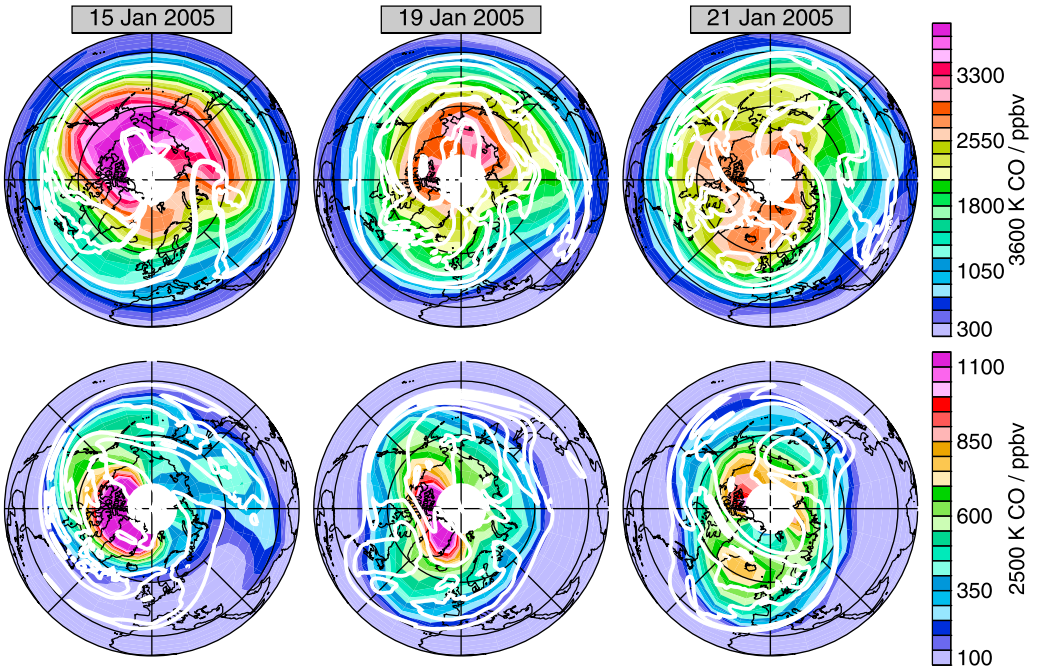

Figure 4. Northern Hemisphere CO mixing ratios. The data are daily averages of MLS observations at potential temperature surfaces of 2500 K (~60 km) and 3600 K (~63 km) presented in a 5° × 15° latitude-longitude grid. The superimposed white lines are PV contours presented exactly as in Figure 3.

clusters with HNO_3. In either case, reaction (1) leads to net production of one HNO_3 molecule. There exists a related pathway in which reaction (4) is substituted by the following reactions, having the same net effect:

$$O_2^- + O_2 + M \rightarrow O_4^- + M \quad (7)$$

$$O_4^- + CO_2 \rightarrow CO_4^- + O_2 \quad (8)$$

$$CO_4^- + O_3 \rightarrow O_3^- + CO_2 + O_2 \quad (9)$$

[22] These two pathways together explain more than 60% of the NO_3^- production from NO_x. Another pathway, producing NO_3^- from NO instead of NO_2, is the following one:

$$e^- + O_2 + O_2 \rightarrow O_2^- + O_2$$

$$O_2^- + O_3 \rightarrow O_3^- + O_2$$

$$O_3^- + CO_2 \rightarrow CO_3^- + O_2$$

$$CO_3^- + NO \rightarrow NO_2^- + CO_2 \quad (10)$$

$$NO_2^- + O_3 \rightarrow NO_3^- + O_2 \quad (11)$$

$$\text{Net}: e^- + NO + 2O_3 \rightarrow NO_3^- + 2O_2.$$

[23] Again there exists a related pathway in which reaction (4) is substituted by the reactions (7)–(9). These two pathways contribute more than 20% to the NO_3^- production from NO_x.

[24] The reactions in the above-listed pathways are prime candidates for reactions influencing the mixing ratio of HNO_3 (theoretically, also reactions influencing the reactants in (3)–(11) might be of importance). That is why we conducted a search of their published rate constants and found that a substantial revision of the rate coefficients of reactions (6) and (10) is justified by the laboratory measurements of *Arnold et al.* [1995]. The new coefficients are $1.3 \times 10^{-11} \times (300/T)^{1.64}$ and $3.3 \times 10^{-11} \times (300/T)^{2.38}$ cm^3 s^{-1}, respectively, where T is temperature. Compared to the coefficients previously used in the model, the new ones are ~70% smaller around 60 km altitude. This leads to a substantial reduction in HNO_3 production and also to much better agreement with satellite observations, as we will show in section 6.

[25] With the revised model, we simulated the two SPEs using the GOES-11 proton flux observations to calculate ionization rates. MLS temperature and water vapor were averaged over the SPE periods and then used in the modeling at 20–85 km instead of those provided by MSISE-90, giving a more realistic representation. Also, the neutral density was calculated from MLS temperature and pressure using the ideal gas law, and then used in the modeling. Because of the significantly coarser altitude resolution of the observations, the model results were made comparable to MLS data by applying the 190-GHz averaging kernels shown in Figure 2 (left). The spectral signature of HNO_3 at the altitudes considered here is somewhat weak in comparison to the noise on the MLS radiances. Accordingly, the sensitivity of the MLS HNO_3 product at these altitudes is reduced from that in the recommended altitude range, and a significant fraction of the information on HNO_3 derives from an a priori climatology field that assumes less than

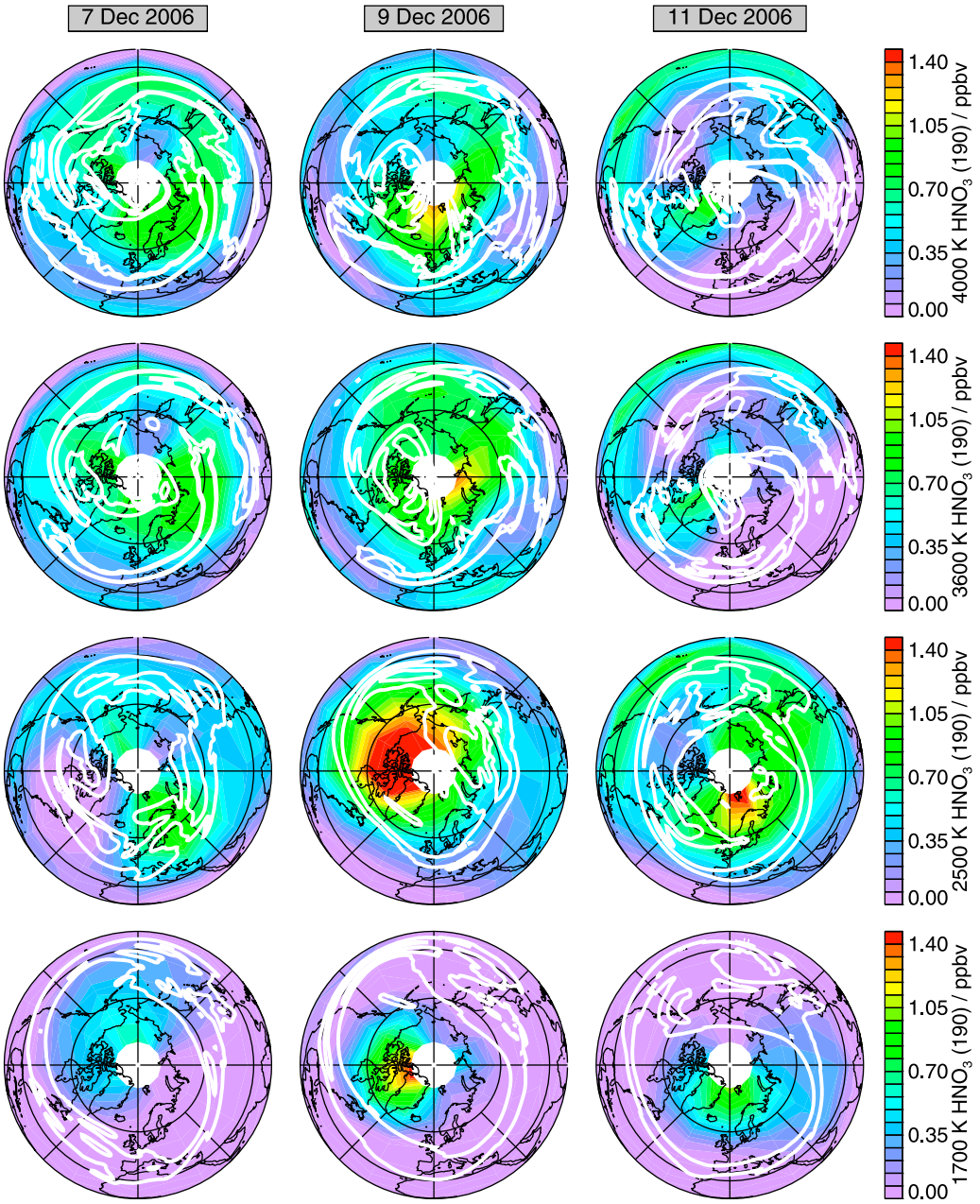

Figure 5. Same as Figure 3 but for December 2006.

1 pptv at these altitudes. The averaging kernel effectively reports the fraction of the information in a product obtained from the MLS observations, and applying the kernel to the model results yields the profiles that MLS would be expected to record were the atmosphere in the state indicated by the model. For more details about the MLS averaging kernels, see *Livesey et al.* [2011]. In the case of HNO_3 enhancement, consideration of averaging kernels significantly decreases the modeled mixing ratios above 55 km, and increases them at 40–55 km. A typical example of these effects is shown in Figure 2 (right). This example demonstrates clearly that the modeled mixing ratio peak at about 82 km, which is due to the combination of increase in NO and decrease in H_2O with increasing altitude, cannot be resolved from MLS data.

5. Distribution of Mesospheric HNO_3 During the SPEs

[26] In the mesosphere, the distribution of HNO_3 in the polar night regions during an SPE is governed by two main processes: (1) production by SPE-related ion chemistry, with the effects typically covering the whole polar region above a certain magnetic latitude (about 60°); and (2) loss related to atmospheric dynamics, i.e., transport to regions affected by photodissociation and mixing with air unaffected

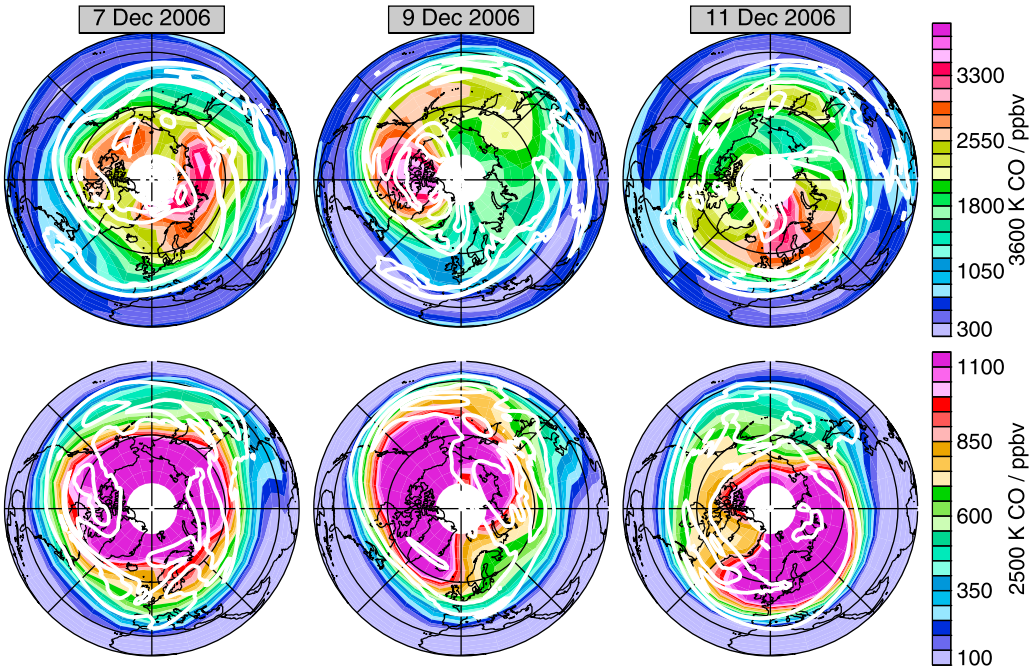

Figure 6. Same as Figure 4 but for December 2006.

by the SPE, which eventually lead to decreases in the amount of SPE-produced HNO_3. Our 1-D modeling can be used to investigate process 1 but neglects process 2. For this reason, we first examine the Northern Hemisphere latitude-longitude distribution of the observed HNO_3 increase in order to understand the spatial behavior of HNO_3 within the polar cap region during the SPEs.

[27] Figure 3 shows the daily mean HNO_3 mixing ratios as observed by MLS on 15, 19, and 21 January 2005, at altitudes between about 50 and 65 km (1700–4000 K in potential temperature). The 15 January data show the conditions before the onset of the SPE. At all altitudes, there is less than 1 ppbv HNO_3 present in the mesosphere, i.e., a relatively small amount compared to the typical peak lower-stratospheric values of ~10 ppbv. On 19 January, right after the main peak of proton forcing, the impact of the SPE is clear at all altitudes as elevated HNO_3 mixing ratios are observed throughout the polar regions, at latitudes higher than about 60°. On 21 January, a few days after the main peak of the SPE, the distribution of the high HNO_3 mixing ratios has changed compared to 19 January. High polar region values are still observed at 50–60 km, although the longitude coverage is slightly different, while the amount of HNO_3 has decreased significantly at 63–65 km.

[28] The CO and PV data at about 60 and 63 km (at 2500 and 3600 K) in Figure 4 can be used to understand the behavior of HNO_3. The CO values on 19 and 21 January are lower than those on earlier days (including 15 January shown in Figure 4). Also, the PV fields are more fragmented and filamentary than on earlier days. This suggests that the air within the vortex region experienced more mixing during the days at and following the peak of the SPE event, leading to rapid reduction of high CO (and HNO_3) values. At 60 km, there is a patch of low CO along with a tongue of low PV gradually (beginning on 19 January) entering the polar region from 60°W direction, eventually extending from 60°W to 45°E and splitting the high-CO region on 21 January. This is an indication that at that altitude, there may have been a large filament of outside-vortex air transported over that region.

[29] Figure 5 presents the HNO_3 polar data in December 2006. In this case, 7, 9, and 11 December correspond to the situation before, right after, and a few days after the main peak of SPE forcing, respectively. The data show quite similar features to what was observed in January 2005. First, there is less than 1 ppbv of HNO_3 present in the polar regions before the SPE. Then, right after the peak forcing high HNO_3 values are seen, especially above latitude 60°N. Finally, a few days afterwards HNO_3 shows a different longitude distribution and lower mixing ratios compared to 9 December.

[30] Figure 6 shows the CO and PV data in December 2006. The PV fields at 63 km are quite filamentary throughout the period, suggesting again that the HNO_3 enhancement might be rapidly mixed with low-HNO_3 air. The CO values are consistent with this: they are lower than on 15 January 2005, when the vortex appears to be more robust. Perhaps even more clearly than in the case of January 2005, a low-CO/low-PV patch is moving toward the polar region from about 45°W on December 11, suggesting that the change in the HNO_3 distribution is primarily a horizontal transport effect.

[31] From Figures 3 and 5 it seems that the distribution of HNO_3 enhancements on 19 January and 9 December contradicts the expectation of homogeneous proton forcing above 60 degrees of magnetic latitude. This could mean that either the proton forcing varied with location in the magnetic polar cap region, or the combination of transport and mixing had significant impact on the HNO_3 distribution already during the SPEs. At least in the case of January 2005 the former option is not plausible, because a recent study by *Bornebusch et al.* [2010] has shown that a homogeneous proton forcing, and thus production of HNO_3, is a valid assumption. On the other hand, the CO and PV data in Figures 3–6 show patterns that are consistent with the HNO_3

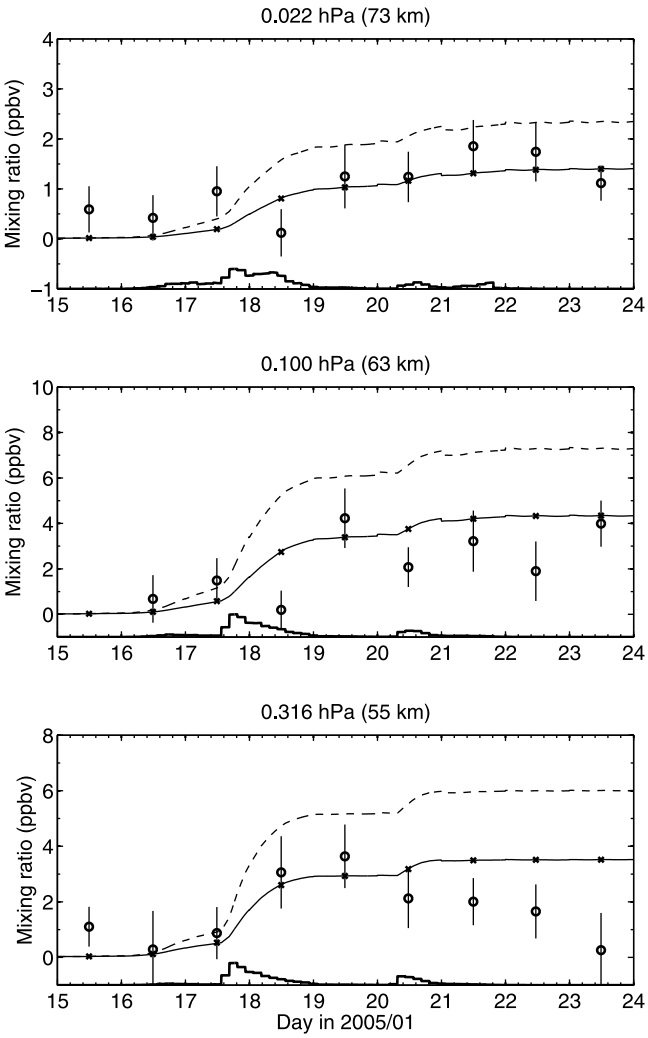

Figure 7. HNO_3 mixing ratios at selected altitudes in January 2005. Circles and corresponding vertical lines mark the daily mean and standard error of the mean of MLS observations, respectively, at 75°N–82°N, 60°W–90°W. Solid line is the SIC model result at 80°N, 75°W (MLS averaging kernels applied). The crosses are daily means of model results sampled at the times of the MLS observations. Dashed line is the result from the earlier version of SIC (MLS averaging kernels applied). Thick solid line in the bottom of each plot is the scaled ionization rate, providing a qualitative indication of proton forcing.

decrease resulting from horizontal transport and mixing, the distinction between the two processes being one of scale: in some cases (i.e., transport) an actual tongue of lower CO values is seen moving toward the polar regions; in others (i.e., mixing) there is an overall decrease in CO that suggests horizontal mixing of higher with lower values on smaller scales. In each case, the PV fields are consistent with this explanation.

[32] Therefore, it follows that the highest mixing ratios observed by MLS at high latitudes are those that are the least affected by the loss due to atmospheric transport and mixing, and thus represent best the production by SPE-related ion chemistry. The fact that the highest HNO_3 mixing ratios were observed at polar night latitudes is an additional justification of this conclusion. Based on Figures 3 and 5, we selected MLS observations at latitudes 75–82°N and longitudes 60–90°W to be compared with modeling at 80°N/75°W. This location corresponds best to the highest mixing ratios of HNO_3 observed on both 19 January and 9 December, and it also coincides with the areas of highest CO values (indicating the polar vortex center region). Obviously, the results of the comparison, which we present in section 6, are strongly affected by this selection because substantially lower amounts of HNO_3 are observed by MLS at other locations. For the same reason, a comparison with zonal mean values would give quite different results. However, we are confident that our approach is justified by the discussion above and allows us to execute the MLS-versus-SIC comparison in a robust way.

6. Model Versus Observations

[33] Figure 7 presents the behavior of HNO_3 mixing ratios in January 2005 at selected mesospheric altitudes. In addition to the SIC model results and daily mean MLS observations, scaled ionization rates are shown to indicate the variations in proton forcing. The model results have similar features at all altitudes: (1) before the SPE the HNO_3 mixing ratios are very low, (2) the main peak of ionization leads to substantial enhancements, and (3) the enhanced values remain until the second peak of ionization leads to further, although moderate, enhancement of HNO_3. Maximum increase is seen at 63 km, where on day 17–18 HNO_3 increases by about 3.5 ppbv, with day 20 contributing an additional 1 ppbv. At 55 and 73 km, the first/second phase enhancements are about 3/1 and 1/0.5 ppbv, respectively. These model results agree reasonably well with the MLS observations, which show very similar enhancements from day 16 to 19. However, on days 20–22 MLS shows a decrease from day 19 over most of the profile, while the modeled values remain the same. As shown in section 5, this difference can be explained by transport and mixing, which cause a redistribution and decrease of HNO_3 in high latitudes between day 19 and 21 (see Figure 3). Our 1-D model can not reproduce such a redistribution but is able to capture the magnitude of the ion chemical production of HNO_3 reasonably well. Note that a detectable SPE signal is present also at 73 km, and there seems to be little change in HNO_3 caused by vortex dynamics after January 19. This might be because the vortex behavior is different at this altitude, which is above the highest level at which GEOS-5 PV data are available.

[34] Figure 8 shows the altitude profiles of HNO_3 on selected days of January 2005. Observational data are daily mean mixing ratios, shown together with the standard error of the mean (SEM), which is typically about 1 ppbv at altitudes between 50 and 75 km. The model results are daily averages of data sampled at the times of the MLS observations. Before the onset of the SPE, on day 16, there is little HNO_3 present at altitudes above 45 km. The observed values do oscillate around zero between ± 0.5 ppbv, but these variation are all within SEM from zero. In contrast, right after the main phase of the SPE, on day 19, both the model and the observations show significant enhancements in the mesosphere. Between 50 and 70 km, the observed HNO_3 mixing ratios are larger than 2 ppbv. Maximum mesospheric values of 4–5 ppbv are measured at 55–65 km. At these altitudes,

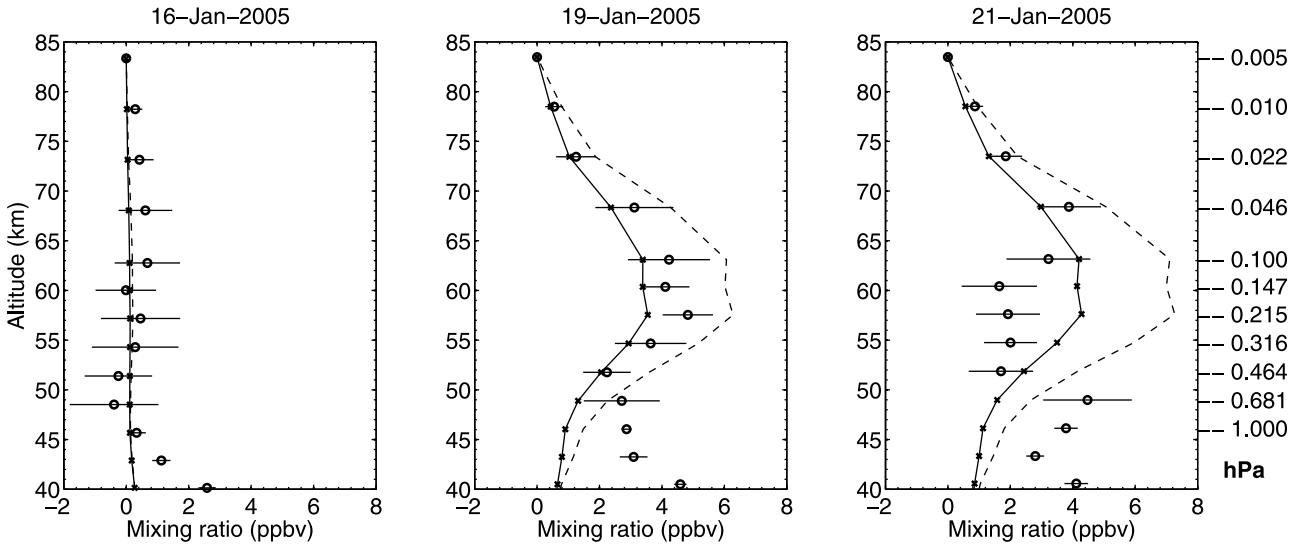

Figure 8. Altitude profiles of HNO_3 mixing ratio in January 2005. Circles and corresponding horizontal lines mark the MLS daily mean and standard error of the mean, respectively, at 75°N–82°N, 60°W–90°W. Solid line is the daily mean of SIC results at 80°N, 75°W sampled at the times of the MLS observations (MLS averaging kernels applied). Dashed line is the result from the earlier version of SIC (MLS averaging kernels applied).

the model results are in reasonable agreement with the observations, correctly predicting the shape but underestimating the magnitude of the enhancement by 0.5–1 ppbv. The difference in mixing ratio between SIC and MLS is in most cases within the SEM of the observations. The agreement between the model and the observations is good also above 70 km, where the observed increase is ≤1 ppbv. Below 50 km, the model shows clearly smaller mixing ratios than the observations (as it does also before the SPE). At these altitudes the results could likely be improved by initializing the model with observations of HNO_3, N_2O_5, and NO_2 [*Verronen et al.*, 2008]. However, we did not pursue this because the focus of this paper is in the mesosphere. A few days after the peak of SPE forcing, on day 21, the effect of atmospheric transport and mixing is seen in the observed profile of HNO_3. Mixing ratios have decreased from those on day 19 by about 2 ppbv at 55–65 km because of the redistribution of HNO_3 in the polar region (see Figure 3). In contrast, the modeled mixing ratios have increased by about 0.8 ppbv due to the second peak of SPE forcing on day 20.

[35] In Figures 7 and 8 we also demonstrate the improvement of HNO_3 production in SIC by showing the results from the previous version of the model. As discussed in section 4, the older version used different reaction rate coefficients of NO_3^- production. At 50–80 km, the revised SIC produces about 40% less HNO_3 during the SPE com-

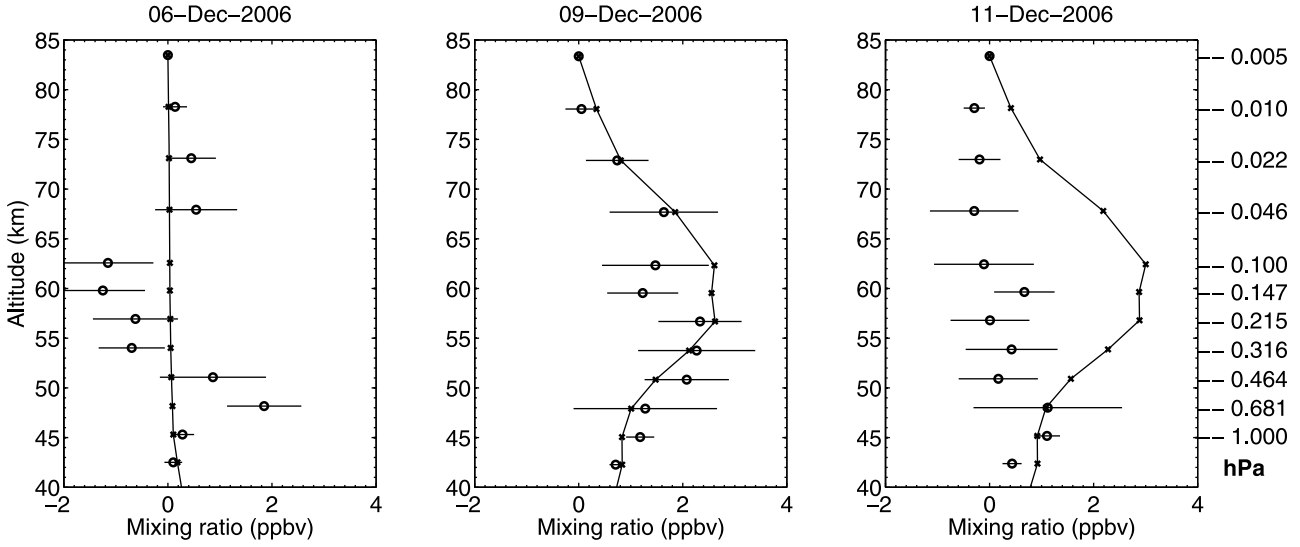

Figure 9. Same as Figure 8 but for December 2006, except that the results from the earlier version of SIC are not shown.

pared to the old version. Therefore, it is clear that the results of the revised model are in better agreement with MLS observations than those from the old version. It should be noted that *Verronen et al.* [2008], who studied the October-November 2003 SPE using the old version of SIC, found that the MIPAS/Envisat instrument observed about 50% less mesospheric HNO_3 in the polar night region compared to the model. Thus, the results of the comparison between MLS and the old version of the model, shown in Figures 7 and 8, are similar to the results of *Verronen et al.* [2008], and give confidence in the mesospheric data quality of both MLS and MIPAS.

[36] The profile comparison for December 2006 is shown in Figure 9. As discussed in section 2, this SPE was smaller in magnitude than the one in January 2005. However, the general behavior of HNO_3 is similar. Before the main peak of the proton forcing, on day 6, both the model and the data show relatively little HNO_3 in the mesosphere. After the main peak of SPE forcing, on day 9, the observed maximum values at 55–65 km are around 2 ppbv and the overall agreement between the model and observations is again reasonably good, although SIC now overestimates the mixing ratios around 60 km by about 1 ppbv. A few days later, on day 11, the transport and mixing have affected HNO_3, leading to a substantial decrease in the observed mixing ratios, this time at all altitudes above 50 km.

7. Conclusions

[37] In this paper, we studied the mesospheric production of HNO_3 during SPEs by comparing the results of the Sodankylä Ion and Neutral Chemistry model with observations from the MLS/Aura instrument. It was shown that our 1-D model, which includes no horizontal transport, can reproduce the observed enhancements of HNO_3 reasonably well. However, careful consideration of the polar vortex dynamics is required so that a proper selection of observations, most suitable to be compared with the model, can be made. The importance of transport and mixing to the HNO_3 distribution in the polar night regions was clearly demonstrated, underscoring the challenges in understanding the SPE-related ionic production of HNO_3 in highly-variable dynamic conditions.

[38] During this work, the SIC model has been revised and improved. Compared to the old version used by, e.g., *Verronen et al.* [2008], the current model predicts about 40% less production of HNO_3 during SPEs. This significantly improves the agreement with observations and gives better confidence in the complex ion chemical scheme of the model.

[39] We showed that the SPEs of January 2005 and December 2006 led to HNO_3 increase of about 4 and 2 ppbv at 50–70 km, respectively. Noting that these SPEs are not among the largest of the recent decades, order-of-magnitude enhancements nevertheless occurred in the mesosphere compared to mixing ratios during quiescent periods. Although in general the MLS HNO_3 observations above 50 km are not recommended for scientific use, this study has shown that during enhancement events, e.g., in the case of SPEs, the MLS HNO_3 data can provide valuable information on the mesosphere.

[40] **Acknowledgments.** The authors would like to thank Nathaniel Livesey for useful comments. The work of P.T.V. and S.M.S. was supported by the Academy of Finland through the projects 136225/SPOC (Significance of Energetic Electron Precipitation to Odd Hydrogen, Ozone, and Climate) and 123275/THERMES (Thermosphere and Mesosphere Affecting the Stratosphere). A.S. was supported by the European Commission through the project FP7-PEOPLE-IEF-2008/237461-EPPIC. P.T.V.'s visit to Jet Propulsion Laboratory in March 2008 was supported by the Vilho, Yrjö, and Kalle Väisälä foundation. Research at the Jet Propulsion Laboratory, California Institute of Technology, is performed under contract with the National Aeronautics and Space Administration. MLS data were provided by the Goddard Earth Sciences Data and Information Service Center.

References

Aikin, A. C. (1997), Production of stratospheric HNO_3 by different ion-molecule reaction mechanisms, *J. Geophys. Res.*, *102*, 12,921–12,925, doi:10.1029/97JD00419.

Arnold, S. T., R. A. Morris, and A. A. Viggiano (1995), Temperature dependencies of the reactions of $CO_3^-(H_2O)_{0,1}$ and O_3^- with NO and NO_2, *J. Chem. Phys.*, *103*, 2454–2458, doi:10.1063/1.469668.

Banks, P. M., and G. Kockarts (1973), *Aeronomy*, Academic, San Diego Calif.

Böhringer, H., D. W. Fahey, F. C. Fehsenfeld, and E. E. Ferguson (1983), The role of ion-molecule reactions in the conversion of N_2O_5 to HNO_3 in the stratosphere, *Planet. Space Sci.*, *31*, 185–191, doi:10.1016/0032-0633(83)90053-3.

Bornebusch, J. P., J. M. Wissing, and M.-B. Kallenrode (2010), Solar particle precipitation into the polar atmosphere and their dependence on hemisphere and local time, *Adv. Space Res.*, *45*, 632–637.

Brühl, C., B. Steil, G. Stiller, B. Funke, and P. Jöckel (2007), Nitrogen compounds and ozone in the stratosphere: Comparison of MIPAS satellite data with the chemistry climate model ECHAM5/MESSy1, *Atmos. Chem. Phys.*, *7*, 5585–5598.

Butkovskaya, N. I., A. Kukui, N. Pouvesle, and G. LeBras (2005), Formation of nitric acid in the gas-phase HO2+NO reaction: Effects of temperature and water vapor, *J. Phys. Chem. A*, *109*, 6509–6520.

Chabrillat, S., G. Kockarts, D. Fonteyn, and G. Brasseur (2002), Impact of molecular diffusion on the CO_2 distribution and the temperature in the mesosphere, *Geophys. Res. Lett.*, *29*(15), 1729, doi:10.1029/2002GL015309.

Degenstein, D. A., N. D. Lloyd, A. E. Bourassa, R. L. Gattinger, and E. J. Llewellyn (2005), Observations of mesospheric ozone depletion during the October 28, 2003 solar proton event by OSIRIS, *Geophys. Res. Lett.*, *32*, L03S11, doi:10.1029/2004GL021521.

de Zafra, R., and S. P. Smyshlyaev (2001), On the formation of HNO_3 in the Antarctic mid to upper stratosphere in winter, *J. Geophys. Res.*, *106*, 23,115–23,126, doi:10.1029/2000JD000314.

Funke, B., et al. (2011), Composition changes after the "Halloween" solar proton event: the High-Energy Particle Precipitation in the Atmosphere (HEPPA) model versus MIPAS data intercomparison study, *Atmos. Chem. Phys. Discuss.*, *11*, 9407–9514, doi:10.5194/acpd-11-9407-2011.

Grenfell, J. L., R. Lehmann, P. Mieth, U. Langematz, and B. Steil (2006), Chemical reaction pathways affecting stratospheric and mesospheric ozone, *J. Geophys. Res.*, *111*, D17311, doi:10.1029/2004JD005713.

Harvey, V. L., C. E. Randall, and M. H. Hitchman (2009), Breakdown of potential vorticity-based equivalent latitude as a vortex-centered coordinate in the polar winter mesosphere, *J. Geophys. Res.*, *114*, D22105, doi:10.1029/2009JD012681.

Heaps, M. G. (1978), The effect of a solar proton event on the minor neutral constituents of the summer polar mesosphere, *Tech. Rep. ASL-TR0012*, U.S. Army Atmos. Sci. Lab., White Sands Missile Range, N. M.

Hedin, A. E. (1991), Extension of the MSIS Thermospheric Model into the Middle and Lower Atmosphere, *J. Geophys. Res.*, *96*, 1159–1172, doi:10.1029/90JA02125.

Jackman, C. H., R. D. McPeters, G. J. Labow, E. L. Fleming, C. J. Praderas, and J. M. Russel (2001), Northern Hemisphere atmospheric effects due to the July 2000 solar proton events, *Geophys. Res. Lett.*, *28*, 2883–2886, doi:10.1029/2001GL013221.

Jackman, C. H., M. T. DeLand, G. J. Labow, E. L. Fleming, D. K. Weisenstein, M. K. W. Ko, M. Sinnhuber, and J. M. Russell (2005), Neutral atmospheric influences of the solar proton events in October-November 2003, *J. Geophys. Res.*, *110*, A09S27, doi:10.1029/2004JA010888.

Jackman, C. H., et al. (2008), Short- and medium-term atmospheric constituent effects of very large solar proton events, *Atmos. Chem. Phys.*, *8*, 765–785.

Lehmann, R. (2002), Determination of dominant pathways in chemical reaction systems: An algorithm and its application to stratospheric chemistry, *J. Atmos. Chem.*, *41*, 297–314.

Lehmann, R. (2004), An algorithm for the determination of all significant pathways in chemical reaction systems, *J. Atmos. Chem.*, *47*, 45–78.

Livesey, N. J., et al. (2011), EOS MLS Version 3.3 Level 2 data quality and description document version 3.3x-1.0, JPL D-33509, Jet Propul. Lab., Pasadena, Calif.

López-Puertas, M., B. Funke, S. Gil-López, T. von Clarmann, G. P. Stiller, M. Höpfner, S. Kellmann, H. Fischer, and C. H. Jackman (2005a), Observation of NO_x enhancement and ozone depletion in the Northern and Southern Hemispheres after the October-November 2003 solar proton events, *J. Geophys. Res.*, *110*, A09S43, doi:10.1029/2005JA011050.

López-Puertas, M., et al. (2005b), HNO_3, N_2O_5 and $ClONO_2$ enchancements after the October-November 2003 solar proton events, *J. Geophys. Res.*, *110*, A09S44, doi:10.1029/2005JA011051.

Manney, G. L., et al. (2007), Solar occultation satellite data and derived meteorological products: Sampling issues and comparisons with Aura Microwave Limb Sounder, *J. Geophys. Res.*, *112*, D24S50, doi:10.1029/2007JD008709.

Manney, G. L., et al. (2008), The evolution of the stratopause during the 2006 major warming: Satellite data and assimilated meteorological analyses, *J. Geophys. Res.*, *113*, D11115, doi:10.1029/2007JD009097.

Orsolini, Y. J., G. L. Manney, M. L. Santee, and C. E. Randall (2005), An upper stratospheric layer of enhanced HNO_3 following exceptional solar storms, *Geophys. Res. Lett.*, *32*, L12S01, doi:10.1029/2004GL021588.

Orsolini, Y. J., J. Urban, and D. P. Murtagh (2009), Nitric acid in the stratosphere based on Odin observations from 2001 to 2007—Part 2: High-altitude polar enhancements, *Atmos. Chem. Phys.*, *9*, 7045–7052, doi:10.5194/acp-9-7045-2009.

Porter, H. S., C. H. Jackman, and A. E. S. Green (1976), Efficiencies for production of atomic nitrogen and oxygen by relativistic proton impact in air, *J. Chem. Phys.*, *65*, 154–167.

Pumphrey, H. C., et al. (2007), Validation of middle-atmosphere carbon monoxide retrievals from the Microwave Limb Sounder on Aura, *J. Geophys. Res.*, *112*, D24S38, doi:10.1029/2007JD008723.

Reinecker, M. M., et al. (2008), The GEOS-5 data assimilation system: A documentation of GEOS-5.0, *Tech. Rep. 104606 V27*, NASA Goddard Space Flight Cent., Greenbelt, Md.

Rodger, C. J., M. A. Clilverd, P. T. Verronen, T. Ulich, M. J. Jarvis, and E. Turunen (2006), Dynamic geomagnetic rigidity cutoff variations during a solar proton event, *J. Geophys. Res.*, *111*, A04222, doi:10.1029/2005JA011395.

Rohen, G., et al. (2005), Ozone depletion during the solar proton events of October/November 2003 as seen by SCIAMACHY, *J. Geophys. Res.*, *110*, A09S39, doi:10.1029/2004JA010984.

Rusch, D. W., J.-C. Gérard, S. Solomon, P. J. Crutzen, and G. C. Reid (1981), The effect of particle precipitation events on the neutral and ion chemistry of the middle atmosphere—I. Odd nitrogen, *Planet. Space Sci.*, *29*, 767–774.

Santee, M. L., et al. (2007), Validation of the Aura Microwave Limb Sounder HNO_3 measurements, *J. Geophys. Res.*, *112*, D24S40, doi:10.1029/2007JD008721.

Semeniuk, K., J. C. McConnell, and C. H. Jackman (2005), Simulation of the October-November 2003 solar proton events in the CMAM GCM: Comparison with observations, *Geophys. Res. Lett.*, *32*, L15S02, doi:10.1029/2005GL022392.

Seppälä, A., P. T. Verronen, E. Kyrölä, S. Hassinen, L. Backman, A. Hauchecorne, J. L. Bertaux, and D. Fussen (2004), Solar proton events of October-November 2003: Ozone depletion in the Northern Hemisphere polar winter as seen by GOMOS/Envisat, *Geophys. Res. Lett.*, *31*, L19107, doi:10.1029/2004GL021042.

Seppälä, A., M. A. Clilverd, C. J. Rodger, P. T. Verronen, and E. Turunen (2008), The effects of hard-spectra solar proton events on the middle atmosphere, *J. Geophys. Res.*, *113*, A11311, doi:10.1029/2008JA013517.

Shimazaki, T. (1971), Effective eddy diffusion coefficient and atmospheric composition in the lower thermosphere, *J. Atmos. Terr. Phys.*, *33*, 1383–1401.

Shimazaki, T. (1984), *Minor Constituents in the Middle Atmosphere*, *Dev. Earth Planet. Phys.*, vol. 6, D. Reidel, Dordrecht, Netherlands.

Solomon, S., D. W. Rusch, J.-C. Gérard, G. C. Reid, and P. J. Crutzen (1981), The effect of particle precipitation events on the neutral and ion chemistry of the middle atmosphere: II. Odd hydrogen, *Planet. Space Sci.*, *8*, 885–893.

Stiller, G. P., et al. (2005), An enhanced HNO_3 second maximum in the Antarctic midwinter upper stratosphere 2003, *J. Geophys. Res.*, *110*, D20303, doi:10.1029/2005JD006011.

Thomas, L., and M. R. Bowman (1986), A study of pre-sunrise changes in negative ions and electrons in the D-region, *J. Atmos. Terr. Phys.*, *4*, 219–227.

Tobiska, W. K., T. Woods, F. Eparvier, R. Viereck, L. D. B. Floyd, G. Rottman, and O. R. White (2000), The SOLAR2000 empirical solar irradiance model and forecast tool, *J. Atmos. Sol.-Terr. Phys.*, *62*, 1233–1250.

Turunen, E., P. T. Verronen, A. Seppälä, C. J. Rodger, M. A. Clilverd, J. Tamminen, C.-F. Enell, and T. Ulich (2009), Impact of different precipitation energies on NO_x generation during geomagnetic storms, *J. Atmos. Sol. Terr. Phys.*, *71*, 1176–1189, doi:10.1016/j.jastp.2008.07.005.

Verronen, P. T. (2006), Ionosphere-atmosphere interaction during solar proton events, Ph.D. thesis, Univ. of Helsinki, Helsinki. (Available at http://ethesis.helsinki.fi.)

Verronen, P. T., A. Seppälä, M. A. Clilverd, C. J. Rodger, E. Kyrölä, C.-F. Enell, T. Ulich, and E. Turunen (2005), Diurnal variation of ozone depletion during the October-November 2003 solar proton events, *J. Geophys. Res.*, *110*, A09S32, doi:10.1029/2004JA010932.

Verronen, P. T., A. Seppälä, E. Kyrölä, J. Tamminen, H. M. Pickett, and E. Turunen (2006), Production of odd hydrogen in the mesosphere during the January 2005 solar proton event, *Geophys. Res. Lett.*, *33*, L24811, doi:10.1029/2006GL028115.

Verronen, P. T., C. J. Rodger, M. A. Clilverd, H. M. Pickett, and E. Turunen (2007), Latitudinal extent of the January 2005 solar proton event in the Northern Hemisphere from satellite observations of hydroxyl, *Ann. Geophys.*, *25*, 2203–2215.

Verronen, P. T., B. Funke, M. López-Puertas, G. P. Stiller, T. von Clarmann, N. Glatthor, C.-F. Enell, E. Turunen, and J. Tamminen (2008), About the increase of HNO_3 in the stratopause region during the Halloween 2003 solar proton event, *Geophys. Res. Lett.*, *35*, L20809, doi:10.1029/2008GL035312.

von Clarmann, T., et al. (2005), Experimental evidence of perturbed odd hydrogen and chlorine chemistry after the October 2003 solar proton events, *J. Geophys. Res.*, *110*, A09S45, doi:10.1029/2005JA011053.

Waters, J. W., et al. (2006), The Earth Observing System Microwave Limb Sounder (EOS MLS) on the Aura satellite, *IEEE Trans. Geosci. Remote Sens.*, *44*, 1075–1092, doi:10.1109/TGRS.2006.873771.

R. Lehmann, Alfred Wegener Institute for Polar and Marine Research, Telegrafenberg A 43, D-14473 Potsdam, Germany. (ralph.lehmann@awi.de)

G. L. Manney and M. L. Santee, Jet Propulsion Laboratory, 4800 Oak Grove Dr., Pasadena, CA 91109, USA. (gloria.l.manney@jpl.nasa.gov; michelle.l.santee@jpl.nasa.gov)

S.-M. Salmi and P. T. Verronen, Earth Observation, Finnish Meteorological Institute, PO Box 503 (Erik Palménin aukio 1), FI-00101 Helsinki, Finland. (sanna-mari.salmi@fmi.fi; pekka.verronen@fmi.fi)

A. Seppälä, British Antarctic Survey, NERC, High Cross, Madingley Road, Cambridge CB3 0ET, UK. (annika.seppala@bas.ac.uk)